DYNAMIC ANALYSIS FOR CIRCULAR INCLUSION NEAR INTERFACIAL CRACK IMPACTED BY SH-WAVE IN HALF SPACE

H. Qi J. Yang [*] **Y. Shi**

College of Aerospace and Civil Engineering
Harbin Engineering University
Harbin 150001, China

J. Y. Tian

Institute of crustal Dynamics
China Earthquake Administration
Beijing 100085, China

ABSTRACT

Complex method and Green's function method are used here to investigate the dynamic analysis for circular inclusion near interfacial crack impacted by SH-wave in bi-material half-space. Firstly, the displacement expression of the scattering wave was constructed which satisfied the free boundary conditions, then Green's function could be constructed, which was an essential solution to the displacement field for an elastic right-angle space with a circular inclusion impacted by out-plane harmonic line source loading at vertical surface. Secondly, crack was made out with "crack-division" technique. Meanwhile, the bi-material media was divided into two parts along the bi-material interface based on the idea of interface "conjunction", and then the vertical surfaces of the two right-angle spaces were loaded with undetermined anti-plane forces in order to satisfy displacement continuity and stress continuity conditions at linking section. So a series of algebraic equations for determining the unknown forces could be set up through continuity conditions and the Green's function. Finally, some examples and results for dynamic stress concentration factor of the circular elastic inclusion were given. Numerical results show that they are influenced by interfacial crack, the incident wave number and the free boundary in some degree.

Keywords: Interfacial crack, Circular inclusion, Right-angle space, Green's function, Dynamic stress Concentration factor (DSCF).

1. INTRODUCTION

Generally, it is hard to avoid various defects when working with the manual materials and structures, especially near the interface, such as interfacial crack and circular hole. Meanwhile, crack is always mentioned and investigated in the models of fracture mechanics because of its specificity [1-2]. And the interface is the part where the crack defect always occurs considering the material containing the interface. For example, it is difficult to avoid the crack defect when paste two kinds of material. So many references which investigate the problem of the interfacial crack have been obtained in recent decades [3-5]. Meanwhile, the materials containing the non-crack defects will cause the phenomena of dynamic stress under the dynamic load, and then they may be destroyed in some conditions. So it is significant to investigate the combined defects of crack and non-crack to satisfy the theoretical and the engineering needs. In recent years, a lot of researches in this field have been carried out, and many valuable results have been obtained [6-15]. According to the references, more attentions were paid to global space interfacial problems, but few efforts were given to the problems of bi-material interface in half space. Although the references [14] and [15] have discussed the effects of the cracks on the circular inclusion or cavity, both of them are in the uniform medium. And the Green functions which were constructed are the displacement solution of out-of-plane line source at the arbitrary point in the elastic global space and the right-angle space respectively which are different from the Green function of this paper. In this article, we have investigated the dynamic analysis for circular inclusion near interfacial crack impacted by SH-wave in half space, and the dynamic stress concentration factor around the edge of the circular elastic inclusion is given. In the terms of the solution of SH-wave scattering by a circular inclusion, the material is divided into two parts along y-axis, and the Green's function is an essential solution to the displacement field for an elastic right-angle space with a circular inclusion impacted by out-plane harmonic line source loading at vertical surface. At the same time, a series of algebraic equations for determining the unknown forces could be set up by the idea of interfacial "conjunction". From the numerical results of the dynamic stress concentration factor, we can see that they are influenced by interfacial crack, the incident wave number and the free boundary.

[*] Corresponding author (yangjie04024218@163.com)

DOI : 10.1017/jmech.2012.15
Copyright © 2012 The Society of Theoretical and Applied Mechanics, R.O.C.
https://doi.org/10.1017/jmech.2012.15 Published online by Cambridge University Press

2. CONSTRUCTION OF GREEN'S FUNCTION

The model of SH-wave is the simplest one among the scattering problems of elastic wave, and it only has anti-plane displacement along z axis when the medium impacted by SH-wave. Introducing complex variables $z = x + iy$, $\bar{z} = x - iy$, the relation between displacement function $W(z, z_0)$ and time is $\exp(-i\omega t)$. In complex coordinate system $(z, \bar{z})$, the displacement field of the media satisfies the following governing equation:

$$\frac{\partial^2 W}{\partial z\, \partial \bar{z}} + \frac{1}{4}k^2 W = 0 \tag{1}$$

where, $k = \omega/c_s$ is wave number, while ω and $c_s = \sqrt{\mu/\rho}$ are the disturbing circular frequency and the shearing velocity of the media, ρ and μ are the mass body density and the shearing modulus of the media, respectively.

The stresses in polar coordinate system are:

$$\begin{cases} \tau_{rz} = \mu\left(\dfrac{\partial W}{\partial z}e^{i\theta} + \dfrac{\partial W}{\partial \bar{z}}e^{-i\theta}\right) \\ \tau_{\theta z} = i\mu\left(\dfrac{\partial W}{\partial z}e^{i\theta} - \dfrac{\partial W}{\partial \bar{z}}e^{-i\theta}\right) \end{cases} \tag{2}$$

As Fig. 1 shows, Green's function is an essential solution of displacement field for a right-angle plane with a circular elastic inclusion by anti-plane harmonic line source loading $\delta(z - z_{01})$ at vertical surface.

The boundary conditions of the problem are:

$$\begin{cases} \Gamma_1 : \tau_{xz}\,|_{x=d} = \delta(z - z_{01}) \\ \Gamma_2 : \tau_{yz}\,|_{y=h} = 0 \\ \Gamma_3 : \tau_{rz}^{\mathrm{I}}\,|_{r=R} = \tau_{rz}^{\mathrm{III}}\,|_{r=R},\ G^{\mathrm{I}}\,|_{r=R} = G^{\mathrm{III}}\,|_{r=R} \end{cases} \tag{3}$$

where, $\delta(\cdot)$ is Dirac-Delta function and z_{01} is the point where the line force is acting on the vertical surface, G is Green function.

The basic solution G which satisfies the governing Eq. (1) and the above boundary conditions (3) should include two parts of motion: The disturbance by the line source forces $\delta(z - z_{01})$ acting on the vertical surface in a complete elastic right-angle space and the scattering by the circular elastic inclusion. The former is regarded as the incident wave $G^{(i)}$, which satisfies the stress free conditions at the straight boundaries in the right-angle plane without the circular elastic inclusion and can be expressed as follows by the methods of "image" and the multi-polar coordinate transformation mentioned in reference [16], then:

$$G^{(i)}(z, \bar{z}) = \frac{i}{2\mu_1}\left[H_0^{(1)}\left(k_1 \mid z - z_{01}\mid\right) + H_0^{(1)}\left(k_1 \mid z - z_{01}\mid\right)\right] \tag{4}$$

where, $z_{01} = d + i(h - y_0)$, $z_{02} = d + i(h + y_0)$, $H_0^{(1)}(\cdot)$ is Hankel function of the first kind of 0 order. z_{01} and z_{02} represents the position vector of the source point and the image point respectively.

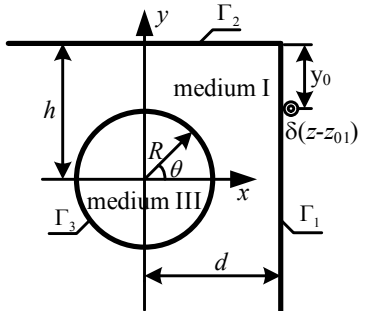


Fig. 1 The right-angle plane model impacted by a line source force

The stresses of Eq. (4) in polar coordinate system are:

$$\begin{cases} \tau_{rz}^{(i)} = -\dfrac{ik_1}{4}(\phi_1 \cdot e^{i\theta} + \phi_2 \cdot e^{-i\theta}) \\ \tau_{\theta z}^{(i)} = \dfrac{k_1}{4}(\phi_1 \cdot e^{i\theta} - \phi_2 \cdot e^{-i\theta}) \end{cases} \tag{5}$$

where

$$\begin{cases} \phi_1 = H_1^{(1)}\left(k_1 \mid z - z_{01}\mid\right)\dfrac{\mid z - z_{01}\mid}{z - z_{01}} + H_1^{(1)}\left(k_1 \mid z - z_{02}\mid\right)\dfrac{\mid z - z_{02}\mid}{z - z_{02}} \\ \phi_2 = H_1^{(1)}\left(k_1 \mid z - z_{01}\mid\right)\dfrac{z - z_{01}}{\mid z - z_{01}\mid} + H_1^{(1)}\left(k_1 \mid z - z_{02}\mid\right)\dfrac{z - z_{02}}{\mid z - z_{02}\mid} \end{cases}$$

The scattering of the circular elastic inclusion will reflect so many times between the circular elastic inclusion and the free boundaries of the right-angle plane that it is difficult to get the scattering wave field which satisfies the stress free conditions at the two straight boundaries. In order to overcome the difficulty, the scattering wave can be expressed by the methods of "image" and the multi-polar coordinate transformation. Then:

$$G^{(s)}(z, \bar{z}) = \sum_{n=-\infty}^{\infty} A_n \sum_{j=1}^{4} S_n^{(j)} \tag{6}$$

where

$$\begin{cases} S_n^{(1)} = H_n^{(1)}\left(k_1 \mid z_1\mid\right)\left[z_1 / \mid z_1\mid\right]^n \\ S_n^{(2)} = H_n^{(1)}\left(k_1 \mid z_2\mid\right)\left[z_2 / \mid z_2\mid\right]^{-n} \\ S_n^{(3)} = (-1)^n H_n^{(1)}\left(k_1 \mid z_3\mid\right)\left[z_3 / \mid z_3\mid\right]^{-n} \\ S_n^{(4)} = (-1)^n H_n^{(1)}\left(k_1 \mid z_4\mid\right)\left[z_4 / \mid z_4\mid\right]^{n} \\ z_1 = z,\ z_2 = z_1 - 2ih,\ z_3 = z_1 - 2d,\ z_4 = z_2 - 2d \end{cases},$$

and A_n is an unknown coefficient to be determined by the boundary conditions.

The stresses of Eq. (6) in polar coordinate system are:

$$\begin{cases} \tau_{rz}^{(s)} = \dfrac{k_1\,\mu_1}{2}\displaystyle\sum_{n=-\infty}^{\infty} A_n(\phi_{n1} \cdot e^{i\theta} - \phi_{n2} \cdot e^{-i\theta}) \\ \tau_{\theta z}^{(s)} = \dfrac{ik_1\,\mu_1}{2}\displaystyle\sum_{n=-\infty}^{\infty} A_n(\phi_{n1} \cdot e^{i\theta} + \phi_{n2} \cdot e^{-i\theta}) \end{cases} \tag{7}$$

https://doi.org/10.1017/jmech.2012.15 Published online by Cambridge University Press

where

$$\phi_{n1} = H_{n-1}^{(1)}(k_1 \mid z_1 \mid)\left(\frac{z_1}{\mid z_1 \mid}\right)^{n-1} - H_{n+1}^{(1)}(k_1 \mid z_2 \mid)\left(\frac{z_2}{\mid z_2 \mid}\right)^{-n-1} - (-1)^n H_{n+1}^{(1)}(k_1 \mid z_3 \mid)\left(\frac{z_3}{\mid z_3 \mid}\right)^{-n-1} + (-1)^n H_{n-1}^{(1)}(k_1 \mid z_4 \mid)\left(\frac{z_4}{\mid z_4 \mid}\right)^{n-1}$$

$$\phi_{n2} = H_{n+1}^{(1)}(k_1 \mid z_1 \mid)\left(\frac{z_1}{\mid z_1 \mid}\right)^{n+1} - H_{n-1}^{(1)}(k_1 \mid z_2 \mid)\left(\frac{z_2}{\mid z_2 \mid}\right)^{-n+1} - (-1)^n H_{n-1}^{(1)}(k_1 \mid z_3 \mid)\left(\frac{z_3}{\mid z_3 \mid}\right)^{-n+1} + (-1)^n H_{n+1}^{(1)}(k_1 \mid z_4 \mid)\left(\frac{z_4}{\mid z_4 \mid}\right)^{n+1}$$

The standing wave filed which is produced by the circular elastic inclusion can be expressed as:

$$G^{(t)} = \sum_{n=-\infty}^{\infty} B_n J_n(k_3 \mid z \mid)\left(\frac{z}{\mid z \mid}\right)^n \tag{8}$$

where, B_n is unknown coefficient to be determined by the boundary conditions, $k_3 = \omega/c_3$ is wave number in elastic inclusion, ω and $c_3 = \sqrt{\mu_3/\rho_3}$ are the disturbing circular frequency and the shearing velocity of the media, and $J_n(\cdot)$ is Bessel function of the first kind.

The stresses of Eq. (8) in polar coordinate system are:

$$\begin{cases} \tau_{rz}^{(t)}(z, \bar{z}) = \dfrac{\mu_3 k_3}{2} \displaystyle\sum_{n=-\infty}^{\infty} B_n \left[\psi_{n1} \cdot e^{i\theta} - \psi_{n2} \cdot e^{-i\theta}\right] \\ \tau_{\theta z}^{(t)}(z, \bar{z}) = \dfrac{i\mu_3 k_3}{2} \displaystyle\sum_{n=-\infty}^{\infty} B_n \left[\psi_{n1} \cdot e^{i\theta} + \psi_{n2} \cdot e^{-i\theta}\right] \end{cases} \tag{9}$$

where

$$\begin{cases} \psi_{n1} = J_{n-1}(k_3 \mid z \mid) \cdot \left(\dfrac{z}{\mid z \mid}\right)^{n-1} \\ \psi_{n2} = J_{n+1}(k_3 \mid z \mid) \cdot \left(\dfrac{z}{\mid z \mid}\right)^{n+1} \end{cases}$$

In complex coordinate system, the boundary conditions at the circular elastic inclusion $r = R$ can be expressed as:

$$\begin{cases} G^{(i)} + G^{(s)} = G^{(t)} \\ \tau_{rz}^{(i)} + \tau_{rz}^{(s)} = \tau_{rz}^{(t)} \end{cases} \tag{10}$$

So the equations to determinate the unknown quantities A_n, B_n can be obtained as follows:

$$\begin{cases} \displaystyle\sum_{n=-\infty}^{\infty} A_n \xi_{n1} + \sum_{n=-\infty}^{\infty} B_n \eta_{n1} = \zeta_1 \\ \displaystyle\sum_{n=-\infty}^{\infty} A_n \xi_{n2} + \sum_{n=-\infty}^{\infty} B_n \eta_{n2} = \zeta_2 \end{cases} \quad (n = 0, \pm 1, \cdots) \tag{11}$$

where

$$\begin{cases} \xi_{n1} = H_n^{(1)}(k_1 \mid z_1 \mid)\left(\dfrac{z_1}{\mid z_1 \mid}\right)^n + H_n^{(1)}(k_1 \mid z_2 \mid)\left(\dfrac{z_2}{\mid z_2 \mid}\right)^{-n} + (-1)^n H_n^{(1)}(k_1 \mid z_3 \mid)\left(\dfrac{z_3}{\mid z_3 \mid}\right)^{-n} + (-1)^n H_n^{(1)}(k_1 \mid z_4 \mid)\left(\dfrac{z_4}{\mid z_4 \mid}\right)^n \\ \eta_{n1} = -J_n(k_3 \mid z \mid)\left(\dfrac{z}{\mid z \mid}\right)^n \\ \zeta_1 = -\dfrac{i}{2\mu_1}\left[H_0^{(1)}(k_1 \mid z - z_{01} \mid) + H_0^{(1)}(k_1 \mid z - z_{02} \mid)\right] \\ \xi_{n2} = \dfrac{k_1 \mu_1}{2}(\phi_{n1} \cdot e^{i\theta} - \phi_{n2} \cdot e^{-i\theta}) \\ \eta_{n2} = -\dfrac{\mu_3 k_3}{2}\left[\psi_{n1} \cdot e^{i\theta} - \psi_{n2} \cdot e^{-i\theta}\right] \\ \zeta_2 = \dfrac{ik_1}{4}(\phi_1 \cdot e^{i\theta} + \phi_2 \cdot e^{-i\theta}) \end{cases}$$

In order to solve Eq. (11), multiply $\exp(-im\theta)$ at the two sides of Eq. (11), determine and integrate in the interval $(-\pi, \pi)$, then a series of infinite algebraic equations can be written as:

$$\begin{cases} \displaystyle\sum_{n=-\infty}^{\infty} A_n \xi_{mn1} + \sum_{n=-\infty}^{\infty} B_n \eta_{mn1} = \zeta_{m1} \\ \displaystyle\sum_{n=-\infty}^{\infty} A_n \xi_{mn2} + \sum_{n=-\infty}^{\infty} B_n \eta_{mn2} = \zeta_{m2} \end{cases} \quad (m = 0, \pm 1, \cdots) \tag{12}$$

where

$$\xi_{mn1} = \frac{1}{2\pi}\int_{-\pi}^{\pi} \xi_{n1} \cdot e^{-im\theta} d\theta\,,\ \eta_{mn1} = \frac{1}{2\pi}\int_{-\pi}^{\pi} \eta_{n1} \cdot e^{-im\theta} d\theta$$

$$\zeta_{m1} = \frac{1}{2\pi}\int_{-\pi}^{\pi} \zeta_1 \cdot e^{-im\theta}\ d\theta\,,\ \xi_{mn2} = \frac{1}{2\pi}\int_{-\pi}^{\pi} \xi_{n2} \cdot e^{-im\theta} d\theta$$

$$\eta_{mn2} = \frac{1}{2\pi}\int_{-\pi}^{\pi} \eta_{n2} \cdot e^{-im\theta} d\theta\ ,\ \zeta_{m2} = \frac{1}{2\pi}\int_{-\pi}^{\pi} \zeta_2 \cdot e^{-im\theta}\ d\theta$$

The Eq. (12) are the limitless equations which can determinate the unknown coefficients A_n and B_n ($n = 0$, ± 1, ± 2, $\cdots$). In this article, 7 items are selected to meet the pre-given computational accuracy in regard to each of a series item of the above-mentioned infinite algebraic equations.

So the Green's function can be obtained as follows:

$$G(z, z_{01}) = G^{(i)}(z, z_{01}) + G^{(s)}(z, z_{01}) \tag{13}$$

3. THEORETICAL MODEL AND ANALYSIS

Figure 2 shows a circular inclusion, in which radius is R, locates bi-media elastic half space. And the distances from the center of the inclusion to the horizontal surface and bi-material interface are h and d, respectively. There is a crack with the length $2A$ at the

https://doi.org/10.1017/jmech.2012.15 Published online by Cambridge University Press

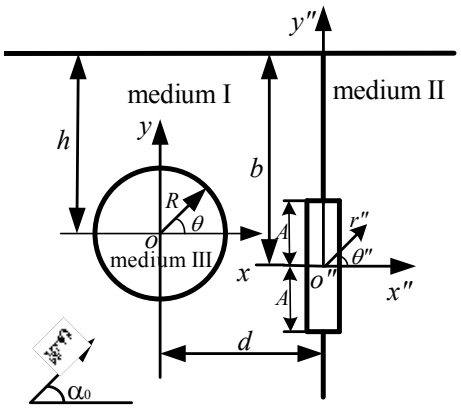


Fig. 2 Bi-material model with an interfacial crack and a circular inclusion in half-space

bi-material interface. And the distance from the center of the crack to the horizontal surface is b. A steady incident SH-wave enters into the half-space from $x'' < 0$ to $x'' = 0$ with the incident angle α_0. Introducing complex system $(z'', \overline{z''})$ in which $z'' = r''\exp(i\theta'')$ and $z'' = z - d + i(b - h)$, where, r'' and θ'' are the polar coordinates in the global coordinate.

Considering the existence of the free boundary, the expression of incident wave can be solved by transforming half-space into global space by the method of "image". Then the equivalent incident wave can be expressed as:

$$W^{(i,e)} = W_0\left\{\exp\left\{\frac{ik_1}{2}\left[z''e^{-i\alpha_0} + \overline{z''}e^{i\alpha_0}\right]\right\} + \exp\left\{\frac{ik_1}{2}\left[(z''-2d)\,e^{-i\beta_0} + (\overline{z''}-2d)\,e^{i\beta_0}\right]\right\}\right\} \tag{14}$$

where, $\beta_0 = \pi - \alpha_0$, α_0 and W_0 are the incident angle and the amplitude of the incident wave respectively.

Similarly, the equivalent refracted wave and the equivalent reflected wave are:

$$W^{(f,e)} = W_1\left\{\exp\left\{\frac{ik_2}{2}\left[z''e^{-i\alpha_4} + \overline{z''}e^{i\alpha_4}\right]\right\} + \exp\left\{\frac{ik_2}{2}\left[(z''-2d)\,e^{-i\beta_1} + (\overline{z''}-2d)\,e^{i\beta_1}\right]\right\}\right\} \tag{15}$$

$$W^{(r,e)} = W_2\left\{\exp\left\{\frac{ik_1}{2}\left[z''e^{i\alpha_0} + \overline{z''}e^{-i\alpha_0}\right]\right\} + \exp\left\{\frac{ik_1}{2}\left[(z''-2d)\,e^{i\beta_0} + (\overline{z''}-2d)\,e^{-i\beta_0}\right]\right\}\right\} \tag{16}$$

where

$$\cos\alpha_1 = (c_2/c_1)\cos\alpha_0\,,$$

$$W_1 = 2W_0\frac{\sin\alpha_0}{\sin\alpha_0 + (\mu_2/\mu_1)(c_1/c_2)\sin\alpha_1}\,,$$

$$W_2 = W_0\frac{\sin\alpha_0 - (\mu_2/\mu_1)(c_1/c_2)\sin\alpha_1}{\sin\alpha_0 + (\mu_2/\mu_1)(c_1/c_2)\sin\alpha_1}\,,$$

$\beta_1 = \pi - \alpha_1$, α_1 is the refraction angle, W_1 and W_2 are the amplitudes of the refracted wave and the reflected wave, respectively.

The expressions of the displacements of the scattering wave field and the standing wave field, which are produced by the circular elastic inclusion impacted by SH-wave, are as the same as the ones produced by the line source forces. The unknown quantities can be determined by the boundary conditions at the circular elastic inclusion, and the methods are also as the same as the process of the solution to the Green's function's.

In order to investigate the dynamic respond of the circular inclusion near the interfacial crack in half-space, the methods of "crack-division" mentioned in reference [14] and interface "conjunction" are used here. As shown in Fig. 3, the detail is as follows: The bi-material media is divided into two parts along the bi-material interface, and a pair of opposite forces with the multitude $[-\tau^{\mathrm{I}}_{\theta''z''}]$ and $[-\tau^{\mathrm{II}}_{\theta''z''}]$ are applied to left and right section of the region where the crack will appear, therefore the resultant force on left (or right) section of the region is zero, which can be thought as crack. At the same time, to satisfy the continuity conditions of stress and displacement in the region outside crack, then a pair of unknown force system $f_1(r_0'', \theta_0'')$ and $f_2(r_0'', \theta_0'')$ must be loaded on the corresponding region of up and down sections. It is obvious that the stress continuity condition is naturally satisfied on the sections.

The total displacements $W^{(\mathrm{I})}$ and stresses $\tau^{(\mathrm{I})}_{\theta''z''}$ at the linking sections are:

$$\begin{cases} W^{(\mathrm{I})} = W^{(i,e)} + W^{(r,e)} + W^{(\mathrm{Is})} \\ W^{(\mathrm{II})} = W^{(f,e)} \\ \tau^{(\mathrm{I})}_{\theta''z''} = \tau^{(i,e)}_{\theta''z''} + \tau^{(r,e)}_{\theta''z''} \\ \tau^{(\mathrm{II})}_{\theta''z''} = \tau^{(f,e)}_{\theta''z''} \end{cases} \tag{17}$$

where, $W^{(\mathrm{Is})}$ are the total displacements of the scattering wave at linking section.

The stress continuity conditions at linking section can be expressed as:

$$\tau^{(\mathrm{I})}_{\theta''z''}\sin\theta_0'' + f_1(r_0'', \theta_0'') = \tau^{(\mathrm{II})}_{\theta''z''}\sin\theta_0'' + f_2(r_0'', \theta_0'') \tag{18}$$

when $\theta_0'' = \beta_2 = -90^{\circ}$, $A \le r_0'' < \infty$, when $\theta_0'' = \beta_3 = 90^{\circ}$, $A \le r_0'' \le b$, and (r_0'', θ_0'') are the arbitrary point at the bi-material interface.

According to $\tau^{(i,e)}_{\theta''z''} + \tau^{(r,e)}_{\theta''z''} = \tau^{(f,e)}_{\theta''z''}$, we can obtain:

$$f_1(r_0'', \theta_0'') = f_2(r_0'', \theta_0'') \quad \theta_0'' = \beta_2, \beta_3 \tag{19}$$

The displacement continuity conditions at interface can be expressed as:

$$W^{(\mathrm{I})} + W^{(f_1)} + W^{(c_1)} = W^{(\mathrm{II})} + W^{(f_2)} + W^{(c_2)} \tag{20}$$

https://doi.org/10.1017/jmech.2012.15 Published online by Cambridge University Press

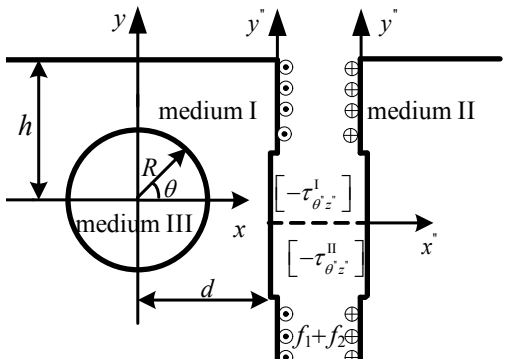


Fig. 3 Conjunction model of bi-material interface in half-space

According to $W^{(i,e)}+W^{(r,e)}=W^{(f,e)}$, we can get:

$$W^{(\mathrm{Is})}+W^{(f_1)}+W^{(c_1)}=W^{(f_2)}+W^{(c_2)} \tag{21}$$

where, $W^{(f_1)}$ and $W^{(f_2)}$ are the displacement fields at an arbitrary point on interface caused by external force system $f_1(r_0'', \theta_0'')$ and $f_2(r_0'', \theta_0'')$, respectively. $W^{(c_1)}$ and $W^{(c_2)}$ are the displacement fields at an arbitrary point on interface caused by external force system $[-\tau^{(\mathrm{I})}_{\theta''z''}]$ and $[-\tau^{(\mathrm{II})}_{\theta''z''}]$, respectively. According to the Green's function which has been obtained and the Eq. (21), the integral equations with undetermined anti-plane forces can be expressed as:

$$\begin{aligned}
&\int_A^b f_1(r_0'', \beta_3)\left[G_1(r'', \beta_3; r_0'', \beta_3)+G_2(r'', \beta_3; r_0'', \beta_3)\right] dr_0'' \\
&\quad+\int_A^\infty f_1(r_0'', \beta_2)\left[G_1(r'', \beta_3; r_0'', \beta_2)+G_2(r'', \beta_3; r_0'', \beta_2)\right] dr_0'' \\
&=\left[-W^{(\mathrm{Is})}\right]_{\theta''=\beta_3}+\int_0^A \tau^{(\mathrm{I})}_{\theta''z''}(r_0'', \beta_2) G_1(r'', \beta_3; r_0'', \beta_2)\, dr_0'' \\
&\quad-\int_0^A \tau^{(\mathrm{I})}_{\theta''z''}(r_0'', \beta_3)\, G_1(r'', \beta_3; r_0'', \beta_3)\, dr_0'' \\
&\quad+\int_0^A \tau^{(\Pi)}_{\theta''z''}(r_0'', \beta_2)\, G_2(r'', \beta_3; r_0'', \beta_2)\, dr_0'' \\
&\quad-\int_0^A \tau^{(\Pi)}_{\theta''z''}(r_0'', \beta_3)\, G_2(r'', \beta_3; r_0'', \beta_3)\, dr_0''
\end{aligned} \tag{22}$$

$$\begin{aligned}
&\int_A^b f_1(r_0'', \beta_3)\left[G_1(r'', \beta_2; r_0'', \beta_3)+G_2(r'', \beta_2; r_0'', \beta_3)\right] dr_0'' \\
&\quad+\int_A^\infty f_1(r_0'', \beta_2)\left[G_1(r'', \beta_2; r_0'', \beta_2)+G_2(r'', \beta_2; r_0'', \beta_2)\right] dr_0'' \\
&=\left[-W^{(\mathrm{Is})}\right]_{\theta''=\beta_2}+\int_0^A \tau^{(\mathrm{I})}_{\theta''z''}(r_0'', \beta_2)\, G_1(r'', \beta_2; r_0'', \beta_2)\, dr_0'' \\
&\quad-\int_0^A \tau^{(\mathrm{I})}_{\theta''z''}(r_0'', \beta_3)\, G_1(r'', \beta_2; r_0'', \beta_3)\, dr_0'' \\
&\quad-\int_0^A \tau^{(\Pi)}_{\theta''z''}(r_0'', \beta_2)\, G_2(r'', \beta_2; r_0'', \beta_2)\, dr_0'' \\
&\quad-\int_0^A \tau^{(\Pi)}_{\theta''z''}(r_0'', \beta_3)\, G_2(r'', \beta_2; r_0'', \beta_3)\, dr_0''
\end{aligned} \tag{23}$$

where, G_1 and G_2 are the Green's functions in media I and II.

The integral equations above are Fredholm equations of the first kind. When the image point and source point of the Green's function coincide, there is singularity of logarithm in the Fredholm equations. Of all methods of solving the equations, direct discrete method is used here. In the light of attenuation characteristic of the scattered wave, the integral equations are transformed into a series of linear algebraic equations to define the added forces $f_1(r_0'', \theta_0'')$ and $f_2(r_0'', \theta_0'')$ at discrete points.

4. NUMERICAL EXAMPLE AND ANALYSIS

Under the effect of the steady incident SH-wave, the dynamic stress concentration factor around the circular inclusion can be expressed as [17]:

$$\tau^*_{\theta z}=|\,\tau^{(\cdot)}_{\theta z}/\tau_0\,| \tag{24}$$

where, $\tau^{(\cdot)}_{\theta z}$ is the stress around the circular elastic inclusion edge, $\tau_0=\mu_1 k_1 W_0$ is the largest amplitude of the incident stresses.

The axial shear stresses around the circular elastic inclusion edge in the right-angle plane I can be expressed as:

$$\begin{aligned}
\tau^{(I)}_{\theta z}=\tau^{(t1)}_{\theta z}&+\int_A^b f_1(r_0'', \beta_3)\frac{\mu_1}{r}\frac{\partial G_1(r, \theta, r_0'', \beta_3)}{\partial\theta}\, dr_0'' \\
&+\int_A^\infty f_1(r_0'', \beta_2)\frac{\mu_1}{r}\frac{\partial G_1(r, \theta, r_0'', \beta_2)}{\partial\theta}\, dr_0''
\end{aligned} \tag{25}$$

where, $\tau^{(t1)}_{\theta z}=\tau^{(i,e)}_{\theta z}+\tau^{(r,e)}_{\theta z}+\tau^{(\mathrm{Is})}_{\theta z}$ at $r = R$ in medium I. It should be point out that the stress at the interfacial boundary point is the nominal value. It is the progressive value instead of the analytic one.

As examples, the dynamic stress concentration factor (DSCF) of the circular inclusion is given. Numerical results are discussed with the effect of interfacial crack, the distance h and the incident wave number k_1R. And they are compared with the informed results. Here, the non-dimensionless parameters $\mu_1^*=\mu_2/\mu_1$, $\mu_2^*=\mu_3/\mu_1$, $k_1^*=k_2/k_1$, $k_2^*=k_3/k_1$.

(1) Figure 4 gives the distribution of the dynamic stress concentration factor $\tau^*_{\theta z}$ around the circular inclusion impacted by SH-wave vertically. Here, $k_1^*=1.0$, $\mu_1^*=1.0$ and $\mu_2^*=0.0$, that is, the example is degenerated into the problem of the uniform media containing a circular hole. The effect of the crack can be ignored when the angle of the incident wave is parallel to the direction of the crack [15]. Meanwhile, the result coincide with the results of the reference [18] when A/R = 1.0, b/R = 12.0, h/R = 12.0 and d/R = 12.0.

(2) Figure 5 gives the distribution of the dynamic stress concentration factor $\tau^*_{\theta z}$ around circular inclusion impacted by SH-wave horizontally.

https://doi.org/10.1017/jmech.2012.15 Published online by Cambridge University Press

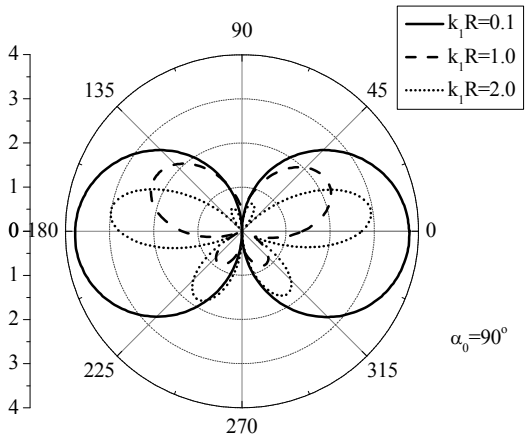
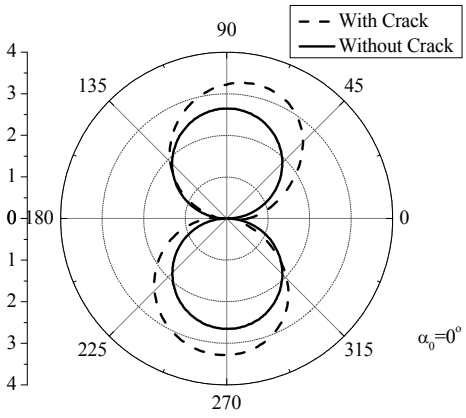
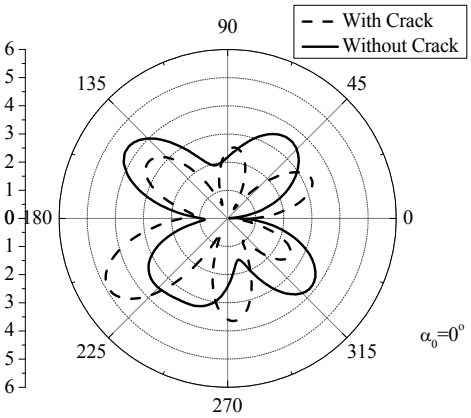


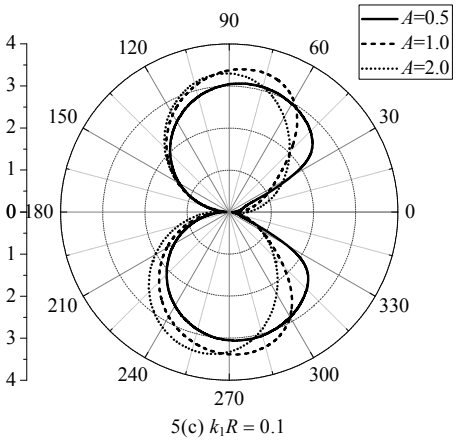
Fig. 4 Distribution of DSCF around hole edge in uniform medium disturbed by SH-wave vertically



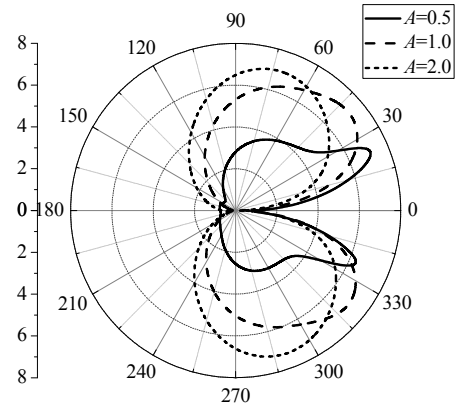
5(a) k_1R = 0.1



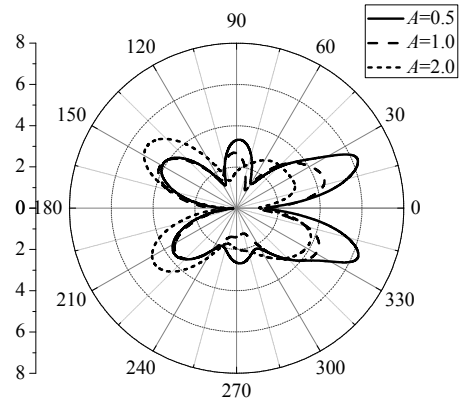
5(b) k_1R = 2.0



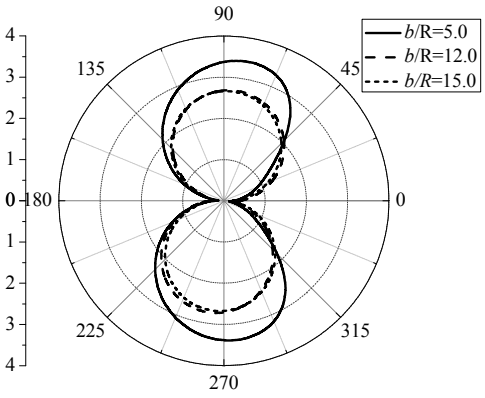
5(c) k_1R = 0.1



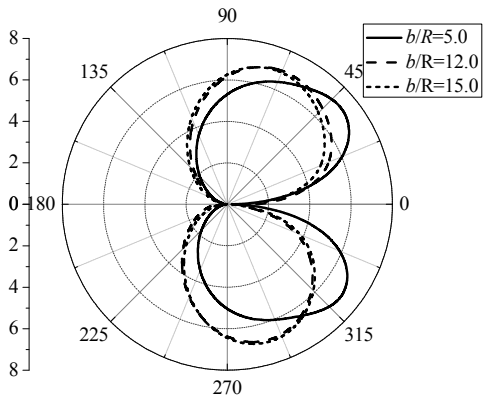
5(d) k_1R = 1.0



5(e) k_1R = 2.0

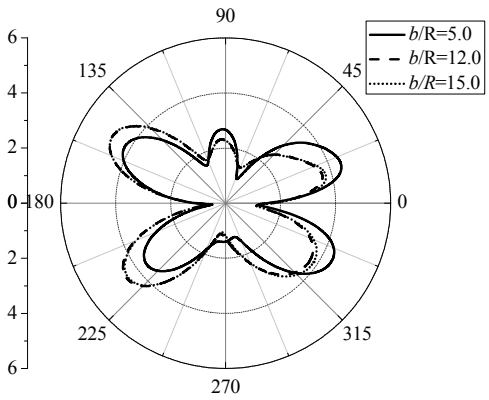


5(f) k_1R = 0.1



5(g) k_1R = 1.0

https://doi.org/10.1017/jmech.2012.15 Published online by Cambridge University Press

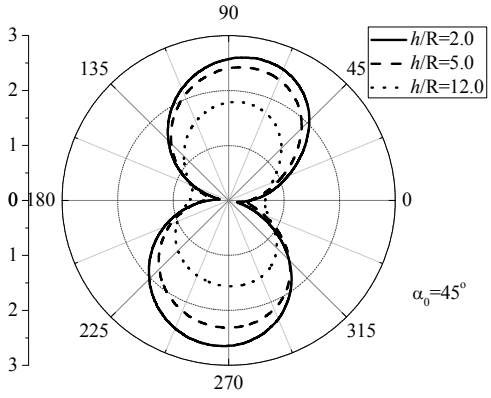


5(h) $k_1R = 2.0$

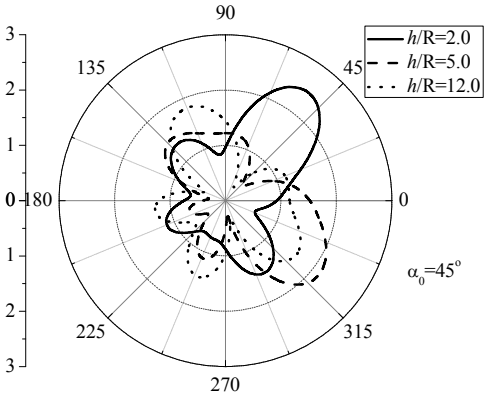
Fig. 5 Distribution of DSCF around inclusion edge in bi-medium disturbed by SH-wave horizontally

Figs. (a) ~ (b) discuss the effect of the existence of the crack on the distributions of DSCF around the circular inclusion. Where A/R = 1.0, b/R = 5.0, d/R = 1.5, h/R = 5.0, $k_1^* = 2.0$, $\mu_1^* = 1.0$, $k_2^* = 2.0$ and $\mu_2^* = 1.0$. When the incident wave number $k_1R = 0.1$, that is the case of "quasi-static", the maximum value of the dynamic stress concentration factor increases over 25% compared with the case of no-crack at the interface. And the dynamic stress concentration changes rapidly when the incident wave enter into the half-space with high frequency, at the same time, the location of the maximum value occur at θ = 210°, and the value increases about 15% compared with the case of no-crack. So the interfacial crack can not be ignored in practical engineering though the above analysis. Figures (c) ~ (e) discuss the effect of the crack lengthon the distributions of DSCF around the circular inclusion. Where b/R = 5.0, d/R = 1.0, h/R = 5.0, $k_1^* = 2.0$, $\mu_1^* = 1.0$, $k_2^* = 2.0$ and $\mu_2^* = 1.0$. From the graphics we can see that the locations of the maximum values trend to the crack tips. However, the sizes of the maximum values do not change significantly. Figures (f) ~ (h) discuss the effect of the crack depth on the distributions of the DSCF around the circular inclusion. Where A/R = 1.0, d/R = 1.0, h/R = 5.0, $k_1^* = 2.0$, $\mu_1^* = 1.0$, $k_2^* = 2.0$ and $\mu_2^* = 1.0$. From the graphics we can see that the graphics of b/R = 12.0 almost coincide with the ones of b/R = 15.0, so the effect of the crack depth can be ignored when the the crack is deep enough.

(3) Figure 6 gives the distribution of the dynamic stress concentration around the circular inclusion impacted by SH-wave aslant. Here, $\alpha_0 = 45°$, A/R = 1.0, b/R = h/R, d/R = 1.5, $k_1^* = 2.0$, $\mu_1^* = 1.0$, $k_2^* = 0.5$ and $\mu_2^* = 1.0$. We can find that the values of the dynamic stress concentration factor are higher when the circular inclusion more



6(a) $k_1R = 0.1$



6(b) $k_1R = 2.0$

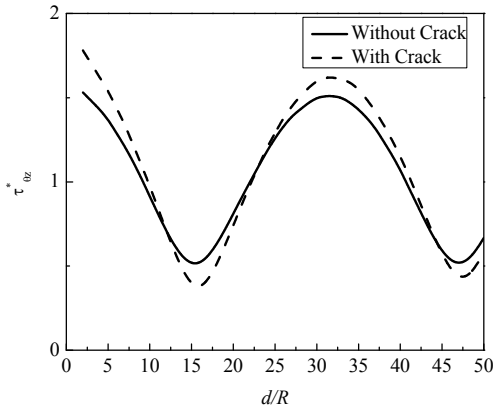
Fig. 6 Distribution of DSCF around inclusion edge in bi-medium disturbed by SH-wave aslant

near to the free surface. When h/R = 2.0 and d/R = 1.5, from the graphics we can see that the maximal value position of DSCF is in 45° direction because of the effects of the free surface and interfacial crack. However, when h/R = 5.0 and 12.0, from the graphics we can see that the maximal value position of DSCF tend to the location of the interfacial crack. That is because the effect of the free surface becomes smaller with the increase of distance h/R and the effect of the interfacial crack plays a leading role.

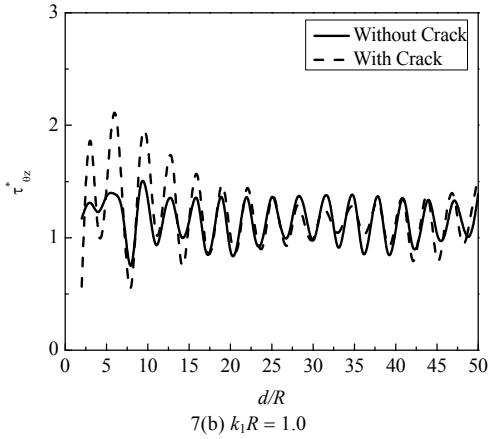
(4) Figure 7 gives the distribution of the dynamic stress concentration of the point θ = 90° around the circular inclusion with the change of the distance d/R. Here, $\alpha_0 = 0°$, A/R = 1.0, b/R = 5.0, h/R = 5.0, $k_1^* = 1.0$, $\mu_1^* = 2.9$, $k_2^* = 1.0$ and $\mu_2^* = 2.9$. From the graphics, we can see that the dynamic stress concentration factor changes periodically with the change of the distance d/R. And the values of the dynamic stress concentration factor are higher when the inclusion is close to the interfacial crack. Meanwhile, the interfacial crack can be ignored when $d/R > 20$.

(5) Figure 8 gives the distribution of the dynamic stress concentration of the point θ = 90° around the circular inclusion with the change of the incident

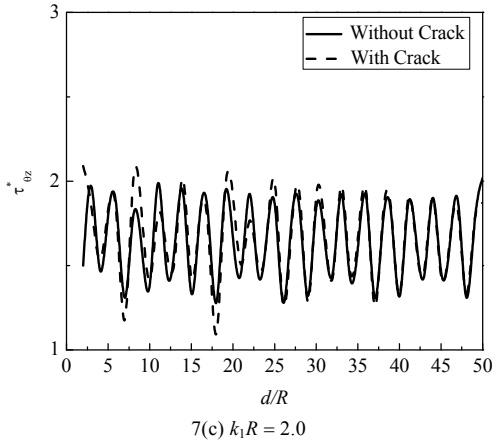
https://doi.org/10.1017/jmech.2012.15 Published online by Cambridge University Press



7(a) $k_1R = 0.1$



7(b) $k_1R = 1.0$



7(c) $k_1R = 2.0$

Fig. 7 Variation of DSCF around circular inclusion edge with d/R

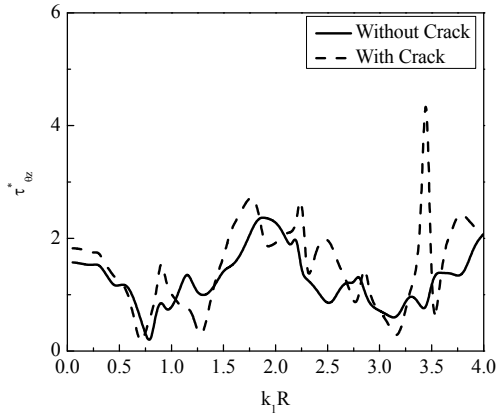


Fig. 8 Variation of DSCF around circular inclusion edge with k_1R

wave number k_1R. Here, $\alpha_0 = 0°$, $A/R = 1.0$, $b/R = 5.0$, $k_1^* = 1.0$, $\mu_1^* = 2.9$, $k_2^* = 1.0$, $\mu_2^* = 2.9$, $d/R = 1.5$ and $h/R = 5.0$. From the graphics, we can see that the dynamic stress concentration factor changes oscillation with the change of the wave number k_1R. And the maximum value of the dynamic stress concentration factor is 5.8 when k_1R appears from 3.0 to 3.5 which the range of the values is 0 to 4.0. However, the maximum value is 2.3 when $k_1R = 2.0$ corresponding to the case of no-crack. So the distribution of dynamic stress concentration factor is influenced by the changes of the incident wave number and the interfacial crack.

5. CONCLUSIONS

In this paper, the complex and Green's function methods are used to discuss the dynamic response problems of a circular inclusion near interfacial crack in half planar space to the steady incident SH-wave. The influences of the interfacial crack, the different distances h and different incident wave number k_1R are studied. The results can provide a theoretical basis in the problems of practical project. The methods used in this paper also adapted to the calculating examples of other media parameters. However, the crack extension will also lead to damage of the structure in some degree, so it is an important task to investigate the dynamic stress concentration near the crack tip. Meanwhile, the authors will investigate the numerical examples of dynamic stress intensity factor near the crack tip in the future because of the specificity of the interfacial crack.

REFERENCES

1. Pedziwiatr, J., "Influence of Internal Cracks on Bond in Cracked Concrete Structures," *Archives of Civil and Mechanical Engineering*, **8**, pp. 91–105 (2008).
2. Yang, S., Song, L. and Li, Z., "Experimental Investigation on Fracture Toughness of Interface Crack for Rock/Concrete," *International Journal of Modern Physics B*, **22**, pp. 6141–6148 (2008).
3. Liu, D. K. and Liu, H. W., "Scattering and Dynamic Stress Concentration of SH-wave by Interface Circular Hole," *Acta Mechanica Sinica*, **30**, pp. 597–604 (1998).
4. Wang, X. D., Zhou Z. Z. and Wang, D., "Impact Response of a Finite Interface Crack," *Explosion and Shock Waves*, **11**, pp. 193–205 (1991).
5. Shi, J. P., Yang, C., Liu, X. H. and Mo, X. Y., "Influence of Inclusions on Bi-materials Interface crack," *Acta Mechanica Sinica*, **36**, pp. 177–183 (2004).

https://doi.org/10.1017/jmech.2012.15 Published online by Cambridge University Press

6. Zhou, Z. G. and Wang, B., "Scattering of Harmonic Anti-plane Shear Waves by an Interface Crack in Magneto_Electro_Elastic Composites," *Applied Mathematics and Mechanics*, **26**, pp. 16–24 (2005).
7. Shi, S. X. and Liu, D. K., "Dynamic Stress Concentration and Scattering of SH-wave by Interface Multiple Circle Canyons," *Acta Mechanica Sinica*, **33**, pp. 60–70 (2001).
8. Liu, D. K. and Lin, H., "Scattering of SH-waves by Circular Cavities near Bimaterial Interface," *Acta Mechanica Solida Sinica*, **24**, pp. 197–204 (2003).
9. Chen, J. T., Chen, C. T., Chen, P. Y. and Chen, I. L., "A Semi-analytical Approach for Radiation and Scattering Problems with Circular Boundaries," *Compute Methods in Applied Methods in Applied Mechanics and Engineering*, **196**, pp. 2751–2764 (2007).
10. Chen, J. T., Chen, P. Y. and Chen, C. T., "Surface Motion of Multiple Alluvial Valleys for Incident Plane SH-waves by Using a Semi-analytical Approach," *Soil Dynamics and Earthquake Engineering*, **28**, pp. 58–72 (2008).
11. Lee, W. M. and Chen, J. T., "Scattering of Flexural Wave in Thin Plate with Multiple Circular Holes by Using the Multiple Trefttz Method," *International Journal of Solids and Structures*, **47**, pp. 1118–1129 (2010).
12. Lee, Vincent W. and Hao, L., "Anti-plane Foundationless Soil-structure Interaction," *Soil Dynamics and Earthquake Engineering*, **30**, pp. 1329–1337 (2010).
13. Guz, A. N. and Zozulya, V. V., "On Dynamical Fracture Mechanics in the Case of Polyharmonic Loading by SH-wave," *International Applied Mechanics*, **46**, pp. 113–119 (2010).
14. Li, H. L. and Liu, D. K., "Dynamic Stress Concentration Problem of SH Wave by Cracks near a Circular Inclusion," *Journal of Harbin Engineering University*, **26**, pp. 359–363 (2005).
15. Qi, H., Shi, Y. and Liu, D. K., "Interaction of a Circular Cavity and a Beeline Crack in Right-angle Plane Impacted by SH-wave," *Journal of Harbin Institute of Technology (New Series)*, **16**, pp. 548–553 (2009).
16. Shi, W. P., Chen, R. P. and Zhang, C. P., "Scattering of Circular Inclusion in Right-angle Plane to Incident Plane SH-wave," *Chinese Journal of Applied Mechanics*, **24**, pp. 154–161 (2007).
17. Pao, Y. H. and Mow, C. C., *Diffraction of Elastic Waves and Dynamics Stress Concentration*, Crane-Russak, New York, 1972.
18. Lin, H. and Liu, D. K., "Scattering of SH-wave around a Circular Cavity in Half Space," *Earthquake Engineering and Engineering Vibration*, **22**, pp. 9–16 (2002).

(Manuscript received October 14, 2010, accepted for publication May 25, 2011.)

https://doi.org/10.1017/jmech.2012.15 Published online by Cambridge University Press